Title	First-principles study of the interplay between grain boundaries and domain walls in ferroelectric PbTiO3
Author(s)	Marton, Pavel; Shimada, Takahiro; Kitamura, Takayuki; Elsaesser, Christian
Citation	PHYSICAL REVIEW B (2011), 83(6)
Issue Date	2011-02
URL	http://hdl.handle.net/2433/161775
Right	©2011 American Physical Society
Type	Journal Article
Textversion	publisher

First-principles study of the interplay between grain boundaries and domain walls in ferroelectric $PbTiO_3$

Pavel Marton,[1] Takahiro Shimada,[2] Takayuki Kitamura,[2] and Christian Elsässer[1,*]
[1]*Fraunhofer-Institut für Werkstoffmechanik IWM, Wöhlerstraße 11, D-79108 Freiburg, Germany*
[2]*Department of Mechanical Engineering and Science, Kyoto University, Sakyo-ku, Kyoto 606-8501, Japan*
(Received 25 November 2010; published 23 February 2011)

Structures and energies of stoichiometric $\Sigma3(111)[\bar{1}10]$, $\Sigma3(112)[\bar{1}10]$, $\Sigma5(201)[010]$, and $\Sigma5(301)[010]$ symmetrical tilt grain boundaries are determined in the tetragonal ferroelectric $PbTiO_3$ using a combination of first-principles electronic-structure calculations and atomistic shell-model-potential simulations. The focus is on grain boundaries, which are ferroelectric domain walls at the same time. A main result is that it is energetically preferential for a 180° domain wall to reside in the region of a $\Sigma5$ grain boundary. This is interpreted as a more general mechanism for domain-wall pinning in polycrystalline ferroelectric materials.

DOI: 10.1103/PhysRevB.83.064110 PACS number(s): 61.72.Mm, 77.80.bn, 77.84.Cg

I. INTRODUCTION

For actuator and sensor applications, ferroelectric perovskite oxides such as $PbTiO_3$ (PTO) or $Pb(Zr,Ti)O_3$ (PZT) are frequently used as functional materials for their superior piezoelectric and dielectric properties. They are often produced in the form of polycrystalline ceramics with relatively fine grain structure (≈5 μm) and even finer ferroelectric domain structure (≈100 nm) appearing within grains, where so-called domain walls create interfaces between regions with differently oriented spontaneous ferroelectric polarization. The large electromechanical response of these materials originates in gradual reversal of spontaneous polarization and spontaneous deformation by shifts of domain walls under external electric fields or mechanical loads. Defects of different types, which are always present in real materials, can pin the domain walls or fix the spontaneous polarization inside the ferroelectric domains, affect the local switching properties, and consequently influence the macroscopic performance of the material. In polycrystalline materials with small grains, the grain boundaries are characteristic structural defects that may provide pinning sites for domain walls. At the same time the mobility of ferroelectric domain walls is considered as a key factor in macroscopic performance of perovskite ferroelectric ceramics. It is therefore interesting to study the interaction of domain walls (DWs) with grain boundaries (GBs) in ferroelectric materials.

Experimental observations of the atomic structure of GBs using high-resolution transmission electron microscopy (HRTEM) revealed atomically sharp interfaces of $\Sigma3$ and $\Sigma5$ GBs in $SrTiO_3$ (Refs. 1–6) (STO) and other perovskites.[7] Boundaries, which appear to be curved and irregular at the macroscale, facet at the microscale in order to decrease the interface energy by creating low-energy boundary segments with low Miller indices.

Theoretical atomic-level studies of GBs in ionic materials are still rare in contrast to metals and semiconductors. This is owing to long-range electrostatic interaction causing mutual interference between interfaces, and consequently requires larger supercells to produce reliable results. Properties of GBs and slip planes in STO (Refs. 8–13) as well as DWs in PTO (Refs. 14–17) were recently studied computationally using first-principles methods of density-functional theory (DFT). In both cases, a very good compliance with existing experimental findings has been found.

The topic of this paper is to study the interplay of GBs with DWs for the case of the tetragonal ferroelectric PTO, which is considered as a model material of the technologically more important PZT. We present a detailed atomic-level study of the $\Sigma3(111)[\bar{1}10]$, $\Sigma3(112)[\bar{1}10]$, $\Sigma5(201)[010]$, and $\Sigma5(301)[010]$ GBs, some of them being DWs simultaneously.

The paper is organized as follows: The details on the first-principles calculations, atomistic simulations, and considered GB structures are given in Sec. II. The main result of our study—interface energies of GBs and their dependence on polarization arrangement in the adjacent grains—is presented in Sec. III. Sections IV and V are devoted to the discussion and to a final conclusion, respectively.

II. METHOD

A. Construction of supercells

For GBs in PTO, an additional complication compared to previous studies of GBs in STO consists in the appearance of spontaneous ferroelectric polarization and tetragonal deformation of the unit cell. Each of the studied interfaces can be a GB and a DW at the same time and may therefore also be mechanically incompatible owing to the different spontaneous ferroelectric strain on either side. It can be pictorially seen in the case of a $\Sigma3(111)[\bar{1}10]$ GB, where the trigonal symmetry perpendicular to the interface present in the cubic phase is broken in the tetragonal phase [an equilateral coincidence-site-lattice (CSL) triangle turns into an isosceles triangle]. Owing to the large spontaneous deformation of PTO,[15] such interfaces could not exist as perfect planes without other structural defects such as dislocations, etc. Therefore, we restrict the considered GB to mechanically compatible interfaces,[18] where the projection of the spontaneous strain tensor to the plane of the GB (DW) is the same for both adjacent grains (domains). Furthermore, we only take into account electrically neutral head-to-tail spontaneous-polarization arrangements in the wall and do not consider charged tail-to-tail or head-to-head walls. It is known that charge-neutral walls (zero net charge across a DW) are electrostatically preferred to charged walls in a perfect material. In the real situation, the charged head-to-head

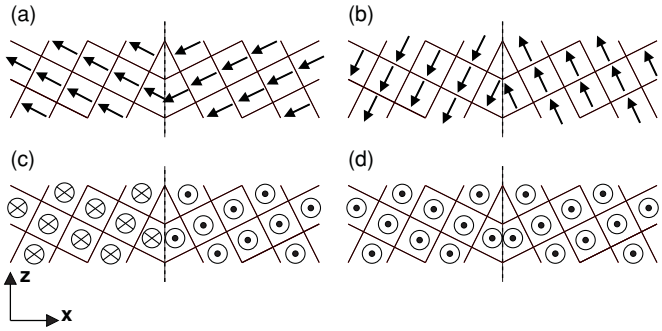

FIG. 1. Schematic sketch of the Σ5(201) grain boundaries with different polarization arrangements in adjacent grains (domains) for supercells with 20 unit cells. (a) 127° DW; (b) 53° DW; (c) 180° DW; (d) 0° polarization change (without a DW). Microscopic translations of grains with respect to each other are disregarded here.

or tail-to-tail domain walls may be compensated by charged defects.

These restrictions lead to just each one possible GB + DW species for the GB Σ3(111) (71° DW) and Σ3(112) (55° DW). The Σ5 GB allow for four interface species, as schematically depicted for Σ5 (201) in Fig. 1. The four DW variants of each Σ5 GB are distinguished in the following by the angle between ferroelectric polarization in the adjacent domains: $\Sigma5(201)^{0^\circ}$, $\Sigma5(201)^{53^\circ}$, $\Sigma5(201)^{127^\circ}$, $\Sigma5(201)^{180^\circ}$, and $\Sigma5(301)^{0^\circ}$, $\Sigma5(301)^{37^\circ}$, $\Sigma5(301)^{143^\circ}$, $\Sigma5(301)^{180^\circ}$. For clarity of the notation, we omit the tilt axis, which is $[\bar{1}10]$ for both Σ3 GBs and [010] for both Σ5 GBs, in the further denomination of interfaces.

The calculations for GBs were performed using atomistic supercells with periodic boundary conditions, where each supercell contains two grains separated by two structurally equal interfaces. For convenience, we introduce a uniquenew coordinate system, which more clearly determines directions with respect to the studied supercell. The x axis is the direction along the long dimension of the supercell perpendicular to the GB plane, and the y axis is $[\bar{1}10]$ for both Σ3 GBs and [010] for both Σ5 GBs. Finally, the z axis complements the local orthogonal coordinate system. The supercells are constructed of 12, 16, 16, and 20 PTO formula units for Σ3(111), Σ3(112), Σ5(201), and Σ5(301), respectively. The number of PTO formula units in each supercell is chosen such that the GBs have approximately same distance of ∼13 Å between interfaces in all considered cases. In addition to this, we also study the Σ3(112) with 18 formula units and Σ5(201) with 20 formula units in order to discuss the convergence of the interface properties with respect to their mutual distance. The equality of the two interfaces in the supercell is guaranteed by a linking operation of symmetry, as summarized in Table I. [The symmetries for Σ3(112) given in Table I hold for the 16-formula-unit supercell. The symmetries for the 18-formula-unit supercell are E, C_{2x}, $m_y + (0,0.5,0)$, and $m_z + (0.5,0.5,0)$.] Owing to the periodicity of the supercell, the studied interfaces do not depend on the choice of a termination plane. One Pb atom in the initial configuration is always placed at $x = 0$ and owing to the symmetry also one at $x = L_x/2$.

TABLE I. Summary of symmetry operations ensuring the equality of the two interfaces in the supercells. The translation part of the symmetry operator is expressed in fractions of the supercell dimensions in the directions (x,y,z). Symmetry operations that are present for all mutual shifts of grains with respect to each other are marked by •. Those that are only present for shifts with a vanishing y component are denoted by ○.

Rotation Translation	E (0,0,0)	C_{2x} (0.5,0,0)	m_y (0,0,0)	m_z (0.5,0,0)
Σ3(111)	•	•	○	○
Σ3(112)	•	•	○	○
$\Sigma5(201)^{0^\circ}$, $\Sigma5(301)^{0^\circ}$	•			•
$\Sigma5(201)^{53^\circ}$, $\Sigma5(301)^{37^\circ}$	•	•	○	○
$\Sigma5(201)^{127^\circ}$, $\Sigma5(301)^{143^\circ}$	•	•	○	○
$\Sigma5(201)^{180^\circ}$, $\Sigma5(301)^{180^\circ}$	•	•		

Some consideration is necessary whether the chosen separation of the GB in the supercell is sufficient to prevent their undesired interaction. This would lead to an inconsistency in comparison with a real material, where the interfaces are much more distant. Meyer and Vanderbilt[14] considered properties of DWs in PTO calculated by DFT for supercells with different DW separations. They showed that the energies of the 180° and 90° domain walls are not fully converged for a DW separation of up to 12 Å, but come quite close to the converged values. Similarly, the properties of GBs in STO were calculated with the supercell setup.[11] For the Σ3(111) a GB separation of 6.68 and 13.36 Å was considered. For Σ3(112), a separation of 9.45 and 18.89 Å was taken into account. In both cases

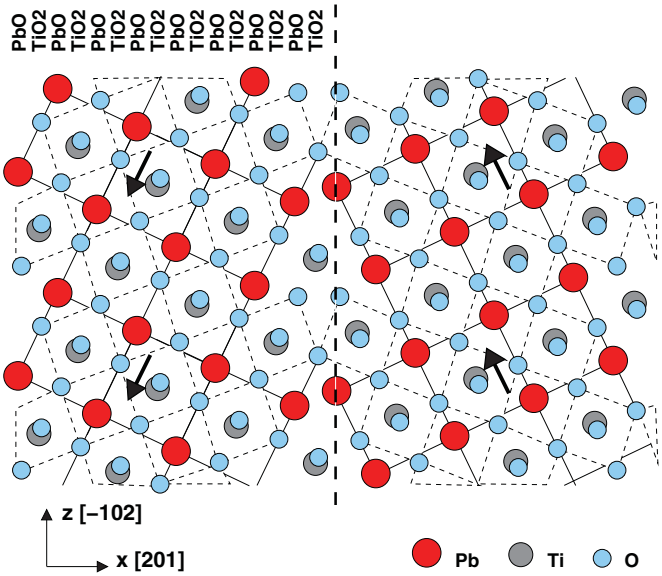

FIG. 2. (Color online) Supercell model of the Σ5(201) GB with a 53° DW, corresponding to the spontaneous-polarization arrangement of Fig. 1(b). The displayed supercell has 16 unit cells (two supercells are plotted in the z direction). The position of the interface is marked by the thick vertical dashed line. Thin solid lines show the shapes of the PTO unit cells. Thin dashed lines indicate the TiO_6 octahedra. The directions of spontaneous polarization are indicated by black arrows. The grains are shifted with respect to each other in this minimum-energy configuration.

the differences in relaxed total energies were rather small, indicating that even the smaller supercells are sufficiently converged with respect to the interface separation. In our study the minimum separation is ∼12 Å for a Σ5(301) GB.

In order to make the structure optimization with large supercells manageable, the structures are prerelaxed using atomistic shell-model-potential simulations, and the positions of atoms are then refined using first-principles DFT calculations.

B. Shell-model-potential simulations

For the classical simulations we use interatomic shell-model potentials (SMPs) as proposed by Dick and Overhauser[19] with Buckingham-type short-range overlap repulsion and van der Waals attraction, electrostatic interaction between cores and shells, and nonlinear springs between each core and its corresponding shell. The shell model provides enough degrees of freedom to properly reproduce the tetragonality of the PTO and atomic displacements, leading to the appearance of a spontaneous ferroelectric polarization. The parametrization by Shimada *et al.*,[15] which we use here, is adjusted to first-principles target data and is therefore suitable for the combined approach of atomistic simulations and first-principles calculations utilized in this work. Moreover, this parametrization proved to yield energies and thicknesses of 180° and 90° domain walls, which are close to those from first-principles DFT calculations.[15] All atomistic simulations with SMP for GBs were conducted using the simulation package GULP.[20] The positions of atoms were relaxed until all forces were smaller than 0.01 eV/Å.

Equilibrium lattice parameters of PTO obtained with the SMP are $a = 3.8535$ Å, $c = 4.0642$ Å, and the fractional z coordinates of positions of atoms in the unit cell are $u_z(\mathrm{Pb}) = 0.0000$, $u_z(\mathrm{Ti}) = 0.5297$, $u_z(\mathrm{O}_1) = 0.6186$, and $u_z(\mathrm{O}_2) = 0.0910$ (cf., e.g., Table 3 in Ref. 23).

C. First-principles DFT calculations

First-principles total energy calculations based on the DFT within the local-density approximation (LDA) were performed using the mixed-basis pseudopotential method (MBPP),[21] employing norm-conserving pseudopotentials[22] and a mixed-basis set[23–26] of plane waves with a cutoff energy of 340 eV, and localized functions. Explicitly treated valence states were $6s$, $5d, 6p$ for Pb, $3s, 3p, 3d$ for Ti, and $2s, 2p, 3d$ for oxygen. The LDA exchange-correlation functional parametrized by Perdew and Zunger[27] was used. The Brillouin-zone integrations were carried out with Monkhorst-Pack meshes[28] appropriate for each particular studied species [with the exception of the Σ3(111) interface, for which a corresponding Moreno-Soler[29] grid was employed]. For all GB calculations, the density of points in the k space roughly corresponds to a $6 \times 6 \times 6$ Monkhorst-Pack k-point mesh of a single-crystal calculation. A 0.2-eV Gaussian broadening was applied.[30] The positions of atoms were relaxed until the forces were less than 0.05 eV/Å.

Both DFT calculations and SMP siumulations were performed with supercells based on equilibrium lattice parameters of PTO determined by DFT-LDA, $a = 3.8558$ Å and $c = 4.0480$ Å. The fractional z coordinates of atoms in the PTO unit cell from DFT-LDA are $u_z(\mathrm{Pb}) = 0.0000$, $u_z(\mathrm{Ti}) = 0.5299$, $u_z(\mathrm{O}_1) = 0.6000$, and $u_z(\mathrm{O}_2) = 0.0917$ (cf., e.g., Table 1 in Ref. 31).

TABLE II. Lateral GB dimensions L_y, L_z and initial GB separation $L_x/2$ perpendicular to the interface for supercells with different numbers of formula units (f.u.). The cross-section area of the supercell is $S = L_y L_z$ [with the exception of Σ3(111), for which $S = (L_y L_z)/2$—cf. Fig. 3(a)] is used in the calculation of the interface energy. The dimension L_x is subsequently optimized, and L_y and L_z are fixed to the given bulk values in the calculations.

GB	f.u.	$L_x/2$ (Å)	L_y (Å)	L_z (Å)	S (Å^2)
$\Sigma3(111)$	12	13.5768	5.4030	9.7611	26.6133
$\Sigma3(112)$	16	13.0011	5.4530	6.7912	37.0322
$\Sigma3(112)$	18	14.6262	5.4530	6.7912	37.0322
$\Sigma5(201)^{0°,180°}$	16	13.7950	4.0480	8.6219	34.9015
$\Sigma5(201)^{53°}$	16	13.9247	3.8558	9.9672	34.5760
$\Sigma5(201)^{127°}$	16	14.3367	5.8558	8.7095	33.5822
$\Sigma5(201)^{0°,180°}$	20	17.2437	4.0480	8.6219	34.9015
$\Sigma5(201)^{53°}$	20	17.4158	3.8558	8.9672	34.5757
$\Sigma5(201)^{127°}$	20	17.9208	3.8558	8.7095	33.5822
$\Sigma5(301)^{0°,180°}$	20	12.1932	4.0480	12.1932	49.3581
$\Sigma5(301)^{37°}$	20	12.2501	3.8558	12.7413	49.1279
$\Sigma5(301)^{143°}$	20	12.7359	3.8558	12.2553	47.2540

The initial dimensions of the considered supercells are summarized in Table II.

D. γ surfaces for grain boundaries

While macroscopically the interface configuration is already determined by specification of the type of GB, the additional microscopic degree of freedom consists in mutual shifts of the two halves of the bicrystal with respect to each other. Some of the shifts are energetically preferred. In order to avoid getting stuck in one of (possibly multiple) local-energy minima,[11] which may appear for different mutual translations of grains, we use SMP simulations to systematically evaluate energies for different shifts, and to determine the energetically most preferred state. The resulting energy maps are known from bulk dislocation simulations as γ surfaces or "generalized stacking faults energy" surfaces.[32,33]

We evaluate the γ surfaces for all four considered interfaces. In the following, the displacement vector $\mathbf{t}$ consists of two components representing y and z components of the shift in fractions of L_y and L_z. For each shift, the bicrystal supercell is constructed and the two grains are displaced rigidly along the interface plane with respect to each other. The initial position $\mathbf{t} = (0,0)$ is defined by the Pb atom in plane $x = 0$ being in $y = 0$ and $z = 0$. Atomic relaxations from this initial configuration are constrained to the direction x perpendicular to the GB plane for atomic cores. Shells are allowed to relax in all directions within the symmetry constraints prescribed in Table I for a particular GB.

Positions of atoms are strongly distorted in the region of a GB, as compared to the perfect crystal. Void spaces appear and also regions with atoms closer to each other than in a perfect structure. Strong repulsion between the close atoms causes the GB to expand perpendicular to the interface. The GB expansion is defined as the excess volume of a GB per unit area. This is taken into account in the calculations by

optimizing the dimension L_x of the supercell perpendicular to the GB simultaneously with relaxation of atomic positions. Dimensions L_y and L_z of the supercell in the GB plane, kept fixed to the bulk values, represent the constraint of the bulk grain. The interface energy of the GB is determined as

$$\gamma = \frac{E_{GB} - E_{bulk}}{2S}, \quad (1)$$

where E_{GB} and E_{bulk} are the total energy of the supercell with the GB and that of the bulk PTO crystal with the same number of formula units, and S is the cross-sectional area of the interface in the supercell. The factor 2 in the denominator reflects the presence of two equivalent interfaces in the supercell.

III. RESULTS

A. γ surfaces for grain boundaries

We first determine the microscopic mutual shift of grains. The obtained γ surfaces for selected variants of GBs are shown in Fig. 3. For the $\Sigma3(111)$ GB there is only one energy minimum for $\mathbf{t} \approx (0,0.05)$ [Fig. 3(a)]. The $\Sigma3(112)$ shows two local minima denoted by "1" for $\mathbf{t} \approx (0,0.05)$ and "2" for $\mathbf{t} \approx (0,0.40)$ [Fig. 3(b)]. This is consistent with theoretical predictions for STO, where two similar minima have been found.[11] In the following we consider the GBs corresponding to both minima. In the case of $\Sigma5(201)^{53^\circ}$ we observe two minima: 1 for $\mathbf{t} \approx (0,0.75)$ and 2 for $\mathbf{t} \approx (0.5,0.02)$ [Fig. 3(c)]. For simplicity, because the GB 2 cannot be made without a DW in the supercell approach (see symmetry considerations below), we restrict our investigation to only the minimum denoted by 1. Finally, both minima, 1 for $\mathbf{t} \approx (0,0.32)$ and 2 for $\mathbf{t} \approx (0,0.90)$, obtained for $\Sigma5(301)^{37^\circ}$ [Fig. 3(d)], are taken into account in the following calculations. Careful inspection of the energy maps reveal some very shallow metastable states in γ surfaces, as, for example, for displacement fractional displacements $\mathbf{t} \approx (0.5,0.6)$ for $\Sigma3(111)$, or $\mathbf{t} \approx (0.5,0.75)$ for $\Sigma5(301)^{37^\circ}$. Both these local minima are more pronounced in the STO simulated with SMP using the parametrization from Ref. 37, and the former was reported, e.g., in Ref. 38. In this work we do not take these shallow minima into account.

The γ surfaces obtained for other variants of the $\Sigma5$ interfaces are qualitatively similar. The minima are shifted slightly along the y axis in the case of the 180° DW, corresponding to the lack of the m_y symmetry [cf. Fig. 1(c)]. In the case of the $\Sigma5$ GB without a DW [Fig. 1(d)] the situation is slightly more complicated. Missing m_y symmetry in this case does not allow to investigate the whole 2D energy surface, but only its 1D profile along the y axis for $\Sigma5(201)^{0^\circ}$ and $\Sigma5(301)^{0^\circ}$. This difference between GBs with and without a 180° DW stems from the fact that while the C_{2x} operation is preserved for all shifts in the y-z plane for the other GB (cf. Table I), in case of both 0° GBs the m_z symmetry relating the two GBs is only present for shifts along the z direction, but is broken for shifts with a nonzero y component. Consequently, the two interfaces are not equivalent for such shifts and cannot be simply treated within the supercell approach. Nevertheless, because for the $\Sigma5$ GB the only minima discussed here are along the z direction, this does not restrict the studied cases any further.

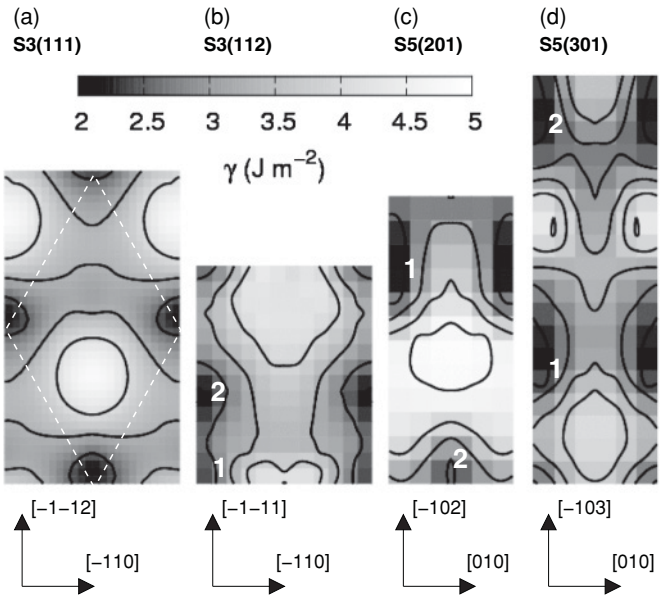

FIG. 3. γ surfaces as obtained from the atomistic SMP simulations. For $\Sigma5$ GB the $(201)^{53^\circ}$ and $(301)^{37^\circ}$ variants are displayed. Lighter gray indicates a higher energy, and darker gray indicates a lower energy (the grayscale is the same for all four plots). Nonequivalent local minima in the energy are referred to in the text by the displayed numbers. The broken lines in $\Sigma3(111)$ indicate the y-z cross-section area of the used supercell.

B. Structure optimization of grain boundaries

Owing to the restriction of the atomic relaxation to the direction perpendicular to the interface, the obtained minimum energies on the γ surfaces give only an estimate of the true positions of atoms at the GBs and their energies. Dimension L_x and positions of atoms for the minimum-energy structures obtained in the preceding procedure were therefore subsequently optimized using the SMP.

Because of the known limitation of SMP to yield quantitatively correct energies,[11,13,35] we further refined the internal coordinates of atoms by means of DFT calculations. The GB separations from the SMP simulations were kept constant. The optimized GB excess expansions (i.e., the change in length with respect to the initial values of $L_x/2$ given in Table II) as well as GB energies obtained using both approaches are given in Table III.

IV. DISCUSSION

From Table III it follows that the atomistic SMP simulations provide only estimates for interface energies, and in general they underestimate the DFT values. Nevertheless, some details of energies, concerning, e.g., different variants of a particular interface, are well reproduced. The SMP-optimized structures were found to be a reasonable approximation for the DFT-optimized structures and accelerated the DFT calculations significantly.

The GB energy of the $\Sigma3(111)$, $\gamma_{SMP} = 143$ mJ m^{-2}, is understimated as compared to $\gamma_{DFT} = 375$ mJ m^{-2}. This value for PTO is smaller than 520 mJ m^{-2} obtained for STO in Refs. 3

TABLE III. Summary of properties of GBs obtained for their different variants and different numbers of formula units (f.u.) in the supercell. SMP-optimized GB excess and interface energies γ evaluated using SMP and DFT are listed.

GB	Variant	f.u.	Excess (Å)	γ_{SMP} (mJ/m^2)	γ_{DFT} (mJ/m^2)
$\Sigma3(111)$		12	0.148	143	375
$\Sigma3(112)$	1	16	0.129	544	683
$\Sigma3(112)$	2	16	0.132	693	1004
$\Sigma3(112)$	1	18	0.138	545	652
$\Sigma3(112)$	2	18	0.139	720	995
$\Sigma5(201)^{0^\circ}$	1	16	0.098	851	1057
$\Sigma5(201)^{53^\circ}$	1	16	0.140	858	963
$\Sigma5(201)^{127^\circ}$	1	16	0.150	731	1080
$\Sigma5(201)^{180^\circ}$	1	16	0.080	836	1069
$\Sigma5(201)^{0^\circ}$	1	20	0.080	908	1114
$\Sigma5(201)^{53^\circ}$	1	20	0.127	875	946
$\Sigma5(201)^{127^\circ}$	1	20	0.161	715	1044
$\Sigma5(201)^{180^\circ}$	1	20	0.081	834	1064
$\Sigma5(301)^{0^\circ}$	1	20	0.273	1067	1266
$\Sigma5(301)^{180^\circ}$	1	20	0.282	1057	1269
$\Sigma5(301)^{0^\circ}$	2	20	0.358	1203	1382
$\Sigma5(301)^{180^\circ}$	2	20	0.377	1150	1326

and 11 with the same method. An expansion of ~0.15 Å per interface agrees well with 0.13–0.17 Å from Ref. 11.

The interface energy of variant 2 of the $\Sigma3(112)$ GB $\gamma_{DFT} = 995$–1004 mJ m^{-2} agrees well with $\gamma_{DFT} = 1040$–1100 mJ m^{-2} of the $\Sigma3(112)(2/3,0)$ GB in Ref. 11, but the interface expansion of ~0.13 Å in PTO is much smaller than ~0.43 Å in STO. The obtained $\gamma_{DFT} = 652$–683 mJ m^{-2} for variant 1 is considerably smaller than the value obtained for variant 2 and also for the corresponding GB in STO, where almost the same energy was reported for both 1 and 2. Surprisingly, the obtained grain expansion of ~0.13 Å for both variants of the $\Sigma3(112)$ GB in PTO is close to 0.14–0.19 Å, reported for $\Sigma3(112)(0,0)$ GB in STO in Ref. 11. The energies from the SMP for $\Sigma3(112)$ in PTO scale well with the DFT values, and a very good agreement is found for both 16- and 18-formula-unit calculations. In variants 1 and 2 of $\Sigma3(112)$ as well as in the case of $\Sigma3(111)$, the interface energy is smaller in PTO than in STO. Apart from different material-specific interactions between atoms, this is probably owing to the lower symmetry of PTO and consequently a less confined structural optimization, leading to lower energies (namely, the mirror-glide plane that is coplanar with the GB in STO is not present in PTO).

Interface energies obtained for a $\Sigma5(201)$ GB turned out to be similar for all studied variants with the exception of $\Sigma5(201)^{53^\circ}$, where the energy calculated with DFT is by ~100 mJ m^{-2} smaller. It is interesting to compare energies of this interface with the 180° DW at the GB and with the DW far away from it. It is remarkable that both SMP simulations and DFT calculations predict a smaller or approximately same energy if the 180° DW lies at the GB compared to the GB without a DW (here denoted as 0°). In order to make the proper comparison of energies of the DW at the GB and far away from it, the energy of the wall must be added to the GB without DW. In Ref. 13 it was shown that the energy of a [100]-oriented 180° DW is $\gamma_{180^\circ} = 132$ mJ m^{-2}. We obtained $\gamma_{180^\circ} = 112$ mJ m^{-2} for a [100]-oriented DW and a similar value of $\gamma_{180^\circ} = 116$ mJ m^{-2} for a [110]-oriented 180° wall. This indicates that the 180° DW in PTO is rather isotropic with respect to the orientation of the DW plane as long as the wall stays electrically neutral. Therefore, it is reasonable to expect that even the energies of the [201] and [301]-oriented 180° DW will be similar. The energy of the [100] 180° DW calculated with the SMP used in this work is $\gamma_{180^\circ} = 139$ mJ m^{-2}. Adding the energy of the 180° DW to the GB without DW leads to even higher energies by ~112 mJ m^{-2} and 139 mJ m^{-2} for configurations with DW outside the GB (DFT and SMP results, respectively).

A very similar tendency was obtained for a $\Sigma5(301)$ GB with and without the 180° DW. The interface energy for the GB without a DW is similar for variant 1 or even larger for variant 2 as the energy of the corresponding interface with the 180° DW. Considering the interface energy of the 180° DW alone, as stated above, it follows that even in this case the DW prefers to stay in the region of the GB.

This consistent behavior of the 180° DW at both $\Sigma5(201)$ and $\Sigma5(301)$ GBs indicates that the presence of a DW at a GB may lead to an even more efficient structure relaxation of the interface. These findings represent perhaps the most interesting result of this study, because they offer a scenario for DW pinning by GBs: If a 180° DW resides in the vicinity of a GB and is free to move (e.g., driven by an external electric field or a mechanical load), its trapping in the region of the $\Sigma5$ GB will lead to an energy gain of the system. Hence, a DW cannot easily escape from the GB after the external driving force is removed. Alternatively, the edges of 180° DWs can be immobilized by a present domain pattern at the $\Sigma5$ GB. Such a scenario, based on a combination of $\Sigma5(201)$ and $\Sigma5(301)$ facets, as observed in STO [cf. Figs. 3(a) and 3(b) in Ref. 4], is sketched in Fig. 4.

In order to discuss the behavior of the spontaneous ferroelectric polarization in the vicinity of the GB+DW, we use formal charges (Pb^{2+}, Ti^{4+}, and O^{2-}) to evaluate the local spontaneous polarization P_s in DFT-optimized configurations. The bulk PTO structure from DFT leads to $P_s = 0.50$ C m^{-2}. This value significantly differs from $P_s = 0.88$ C m^{-2} calculated using the Born effective charges[36] or 0.81 C m^{-2} calculated with the Berry-phase approach,[37] which is owing to the strong underestimation of the dynamical charge of Ti and O atoms in the direction of the tetragonal axis. However, this procedure with the formal charges, which allows only a crude approximation of the real polarization profile, is adopted here in order to facilitate the evaluation of the spontaneous polarization in the strongly deformed unit cells close to the GB, where it is difficult to assign a tetragonal c axis and to attribute relevant Born effective charges to individual atoms. Nevertheless, major features of the polarization profile are sufficiently reproduced even with this simple method.

Owing to a strong distortion of the perovskite structure, it was not possible to evaluate the spontaneous ferroelectric polarization in the core region of the GB itself, but only in adjacent complete perovskite unit cells. The resulting polarization profiles for several GB are displayed in Figs. 5–7.

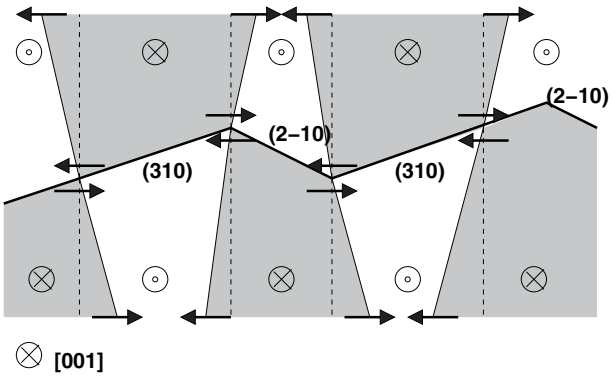

FIG. 4. Possible pinning mechanism of a 180° DW at a GB formed by a combination of Σ5 facets known from STO. The GB forms a DW at the same time along its whole length. An applied external electric field prefers the shaded ferroelectric domains, which grow at the expense of the oppositely oriented domain. Thick solid lines represent the GB, thin dashed lines the original position of the 180° DW, and thin solid lines the shifted DW under influence of the external electric field. Arrows indicate the direction of motion of the DW. If the DWs moved at their crossing point with the GB, a segment of GB without a DW would be created, which is energetically unfavorable. Therefore, the edges of this 180° DW are likely well pinned.

The origin of the x coordinate in the polarization profiles is shifted to the middle of the supercell.

Inspection of the obtained profiles shows that the spontaneous polarization is strongly disturbed in the vicinity of GBs because of strong deformation of the crystallattice.[11] In

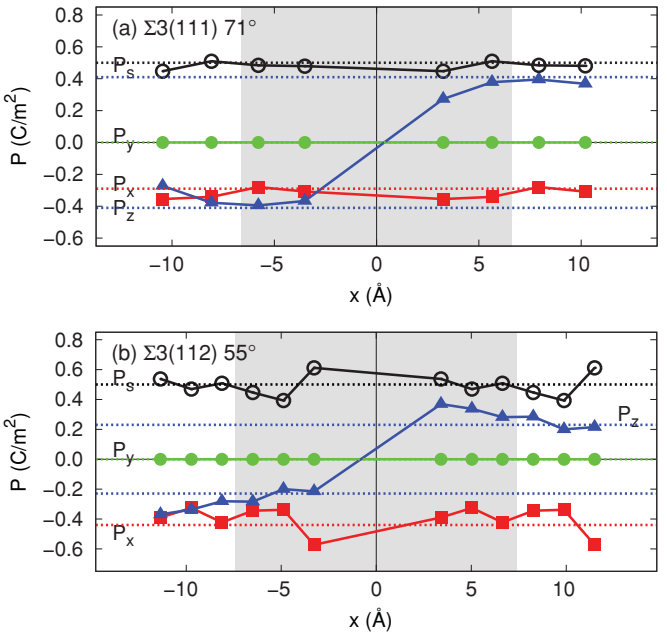

FIG. 5. (Color online) Polarization profiles across (a) the Σ3(111) and b) Σ(112) (variant 2) GBs. Filled squares, circles, and triangles represent the P_x, P_y, and P_z components of spontaneous ferroelectric polarization, respectively. Open circles stand for the magnitude of the spontaneous polarization P_s. The irreducible part of the supercell with the interface in the center ($x = 0$) is marked by shading. Bulk values of P_x, P_y, P_z, and P_s are indicated by thin dotted lines.

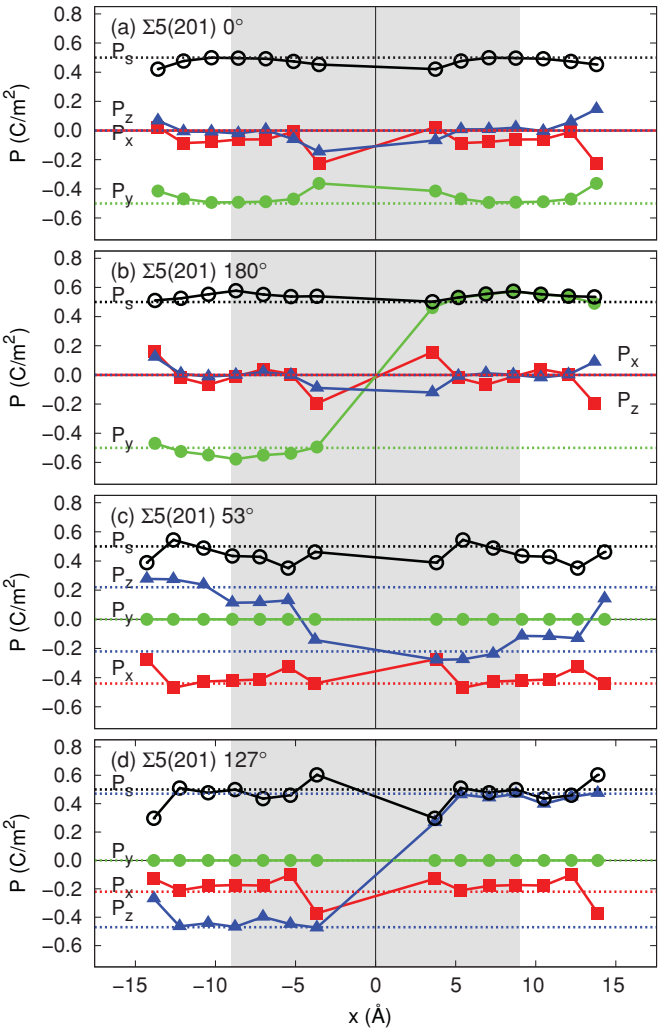

FIG. 6. (Color online) Polarization profiles across the four variants of a Σ5(201) GB in the supercell with 20 unit cells. The symbols used are the same as in Fig. 5.

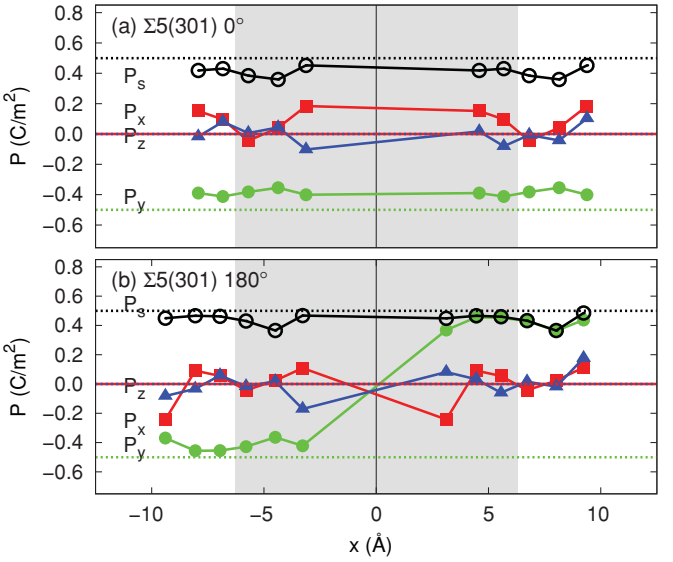

FIG. 7. (Color online) Polarization profiles across variant 2 of the Σ5(301) GB. The symbols used are the same as in Fig. 5.

most cases the ferroelectric polarization approaches its bulk spontaneous modulus and orientation at the center of the grain (domain), although the finite-size effects are still not small [e.g., in Figs. 6(b) and 6(c)]. This is caused by the very small length of dimension L_x of the supercell and by the fact that the L_x is taken directly from SMP simulations and not further refined with the DFT. This may cause an undesired remanent strain in the supercell, leading to a change in ferroelectric polarization, which is quite sensitive to such effects (cf. Ref. 34).

It turned out that for both variants of $\Sigma5(301)^{37^\circ}$ and $\Sigma5(301)^{143^\circ}$ the used grain separation $L_x/2$ is not yet sufficient to produce reliably the structure of the DW. Because the basic features of the γ surface are determined by mutual positions of ions in the GB (cf. Table III) we evaluted this γ surface for STO with a well-tested rigid-ion potential.[11,34] Both γ surfaces for PTO and STO agree well, with the exception that the energy minimum corresponding to $\mathbf{t} \approx (0.5,0.75)$ is more pronounced in STO. Therefore, we are confident that the γ-surface $\Sigma5(301)^{37^\circ}$ in Fig. 3(d) properly describes the energy profile for mutual shifts of grains. Surprisingly, in a DFT study of a $\Sigma5(301)$ GB in STO, Imaeda *et al.*[12] found the most stable configuration in the γ surface for 0.5 Å to shift in direction y. Nevertheless, similar two minima in the m_y symmetry plane were reported, with their distance corresponding well to our results.

Polarization profiles obtained for $\Sigma5(201)$ for supercells with 16 and 20 formula units are plotted on top of each other in Fig. 8. The apparently good agreement between the polarization in both supercells indicates that, despite the fact that the bulk polarization is not exactly attained in the interior of domains between interfaces, the ferroelectric polarization in the vicinity of the GB is already converged reasonably well in the smaller supercell. In the same plot we also compare the polarization from the DFT calculations with that from the SMP simulations. The difference comes mainly from the magnitude of the spontaneous polarization, which is slightly larger for a bulk unit cell optimized with the SMP, coming out as $\sim$0.58 C m^{-2} instead of 0.50 C m^{-2} for the DFT-optimized structure. The results indicate a good agreement between relaxed structures obtained with both methods and hence a good performance of SMP for PTO (Ref. 23) in simulations of the GB.

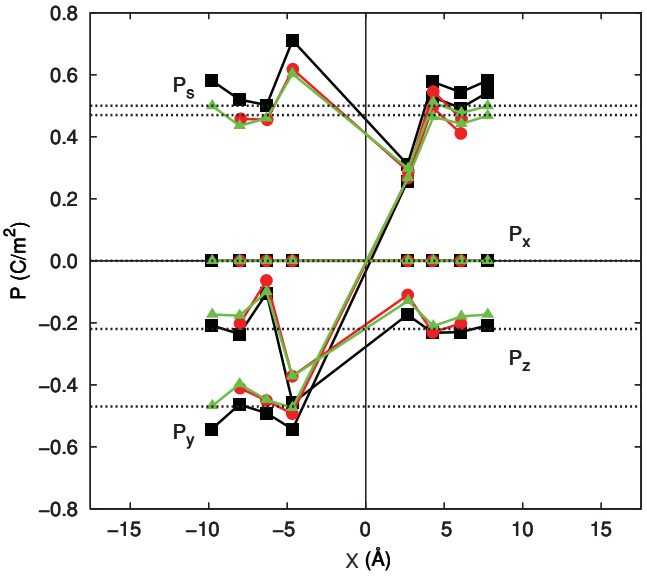

FIG. 8. (Color online) Comparison of the polarization profiles evaluated using DFT in the vicinity of the $\Sigma5(201)$ GB for supercells with 16 formula units (dots, red) and 20 formula units (triangles, green), and using SMP with 20 formula units (squares, black). Results obtained with both SMP and DFT show good agreement.

A possible mechanism for pinning of DWs by GBs has been analyzed and discussed here for particular cases of the 180° DW and the $\Sigma5(201)$ and $\Sigma5(301)$ GB. Nevertheless, it can be expected that the obtained results are indicative of a more general tendency of a DW to get pinned by a GB.

V. CONCLUSION

We have investigated four stoichiometric, electrically neutral, and mechanically compatible symmetrical tilt GBs in tetragonal ferroelectric PTO, namely, $\Sigma3(111)$, $\Sigma3(112)$, $\Sigma5(201)$, and $\Sigma5(301)$ GBs, and their coexistence with ferroelectric DWs. We used the atomistic shell-model-potential simulations to evaluate the γ surfaces, which determine the microscopic translations of grains with respect to each other. Energies of locally (meta)stable GB configurations were further refined by means of DFT calculations. Some (meta)stable configurations, which were identified in the γ surfaces [such as the minimum 2 in the case of $\Sigma3(201)$], were nevertheless disregarded here for simplicity and may be worth investigating further.

The interfaces $\Sigma3(111)$ and $\Sigma3(112)$ in PTO have slightly smaller interface energies than the corresponding interfaces in STO.[3,11] For $\Sigma5(201)$ and $\Sigma5(301)$ it was possible to directly compare energies of a GB with and without a ferroelectric DW. It was shown that the 180° wall energetically prefers to reside at these GBs. The energy gained by trapping of such a DW at a GB is similar to the interface energy of the wall itself. This provides a possible mechanism for pinning of DWs by GBs. Although finite-size effects are not yet fully avoided in the region between interfaces with the employed supercells of still rather small sizes, we are confident that the important aspects of the interplay between GBs and DWs is demonstrated properly with the chosen model supercells and will remain valid for supercells with a larger separation of the GB. The used shell-model-potential parametrization[15] reproduces well the structural properties of GBs in good accordance with the DFT results.

Our results indicate the tendency of extended planar "defects," such as DWs, to be attracted by other structurally extended defects, namely, GBs. Similar behavior is known to determine mechanical and electrical properties of materials via segregation of point defects or pileups of line defects at the GB (e.g., change of conductivity at the GB in STO, embrittlement of metals owing to impurities,[38] or pinning and pileup of lattice dislocations at the GB in metals[39]). We propose this type of pinning mechanism for DWs to be taken into account in future considerations about microscopic origins of the macroscopic properties of ferroelectric perovskite oxides.

ACKNOWLEDGMENTS

This work was funded by the German Federal Ministry of Education and Research (BMBF Framework Programme WING, Project Code 03X0510). It was supported in part by a Grant-in-Aid for Scientific Research (S) (Grant No. 21226005) and a Grant-in-Aid for Young Scientists (B) (Grant No. 21760073) from the Japan Society of Promotion of Science (JSPS).

*christian.elsaesser@iwm.fraunhofer.de

[1] O. Kienzle and F. Ernst, J. Am. Ceram. Soc. **80**, 1639 (1997).
[2] O. Kienzle, M. Exner, and F. Ernst, Phys. Status Solidi A **166**, 57 (1998).
[3] S. Hutt, O. Kienzle, F. Ernst, and M. Rühle, Z. Metallkd. **92**, 105 (2001).
[4] S. B. Lee, W. Sigle, W. Kurtz, and M. Rühle, Acta Mater. **51**, 975 (2003).
[5] S. B. Lee, W. Sigle, and M. Rühle, Acta Mater. **51**, 4583 (2003).
[6] Z. L. Zhang, W. Sigle, F. Phillipp, and M. Rühle, Science **302**, 846 (2003).
[7] O. Eibl, M. Rössel, and N. Peranio (private communication).
[8] S. Hutt, S. Kostlmeier, and C. Elsässer, J. Phys. Condens. Matter **13**, 3949 (2001).
[9] R. Astala and P. D. Bristowe, J. Phys. Condens. Matter **14**, 13635 (2002).
[10] S. Gemming and M. Schreiber, Chem. Phys. **309**, 3 (2005).
[11] N. A. Benedek, Alvin L.-S. Chua, C. Elsässer, A. P. Sutton, and M. W. Finnis, Phys. Rev. B **78**, 064110 (2008).
[12] M. Imaeda, T. Mizoguchi, Y. Sato, H. S. Lee, S. D. Findlay, N. Shibata, T. Yamamoto, and Y. Ikuhara, Phys. Rev. B **78**, 245320 (2008).
[13] P. Hirel, P. Marton, M. Mrovec, and C. Elsässer, Acta Mater. **58**, 6072 (2010).
[14] B. Meyer and D. Vanderbilt, Phys. Rev. B **65**, 104111 (2002).
[15] T. Shimada, K. Wakahara, Y. Umeno, and T. Kitamura, J. Phys. Condens. Matter **20**, 325225 (2008).
[16] T. Shimada, Y. Umeno, and T. Kitamura, Phys. Rev. B **77**, 094105 (2008).
[17] T. Shimada, X. Wang, S. Tomodo, P. Marton, C. Elsässer, and T. Kitamura (accepted for publication, Phys. Rev. B, 2011).
[18] J. Fousek and V. Janovec, J. Appl. Phys. **40**, 135 (1969).
[19] B. G. Dick and A. W. Overhauser, Phys. Rev. **112**, 90 (1958).
[20] J. D. Gale and A. L. Rohl, Mol. Simul. **29**, 291 (2003).
[21] B. Meyer, F. Lechermann, C. Elsässer, and M. Fähnle, FORTRAN90 program for mixed-basis pseudopotential calculations for crystals, Max-Plank Institut für Metallforschung, Stuttgart.
[22] D. Vanderbilt, Phys. Rev. B **32**, 8412 (1985).
[23] C. Elsässer, N. Takeuchi, K. M. Ho, C. T. Chan, P. Braun, and M. Fähnle, J. Phys. Condens. Matter **2**, 4371 (1990).
[24] K. M. Ho, C. Elsässer, C. T. Chan, and M. Fähnle, J. Phys. Condens. Matter **4**, 5189 (1992).
[25] B. Meyer, K. Hummler, C. Elsässer, and M. Fähnle, J. Phys. Condens. Matter **7**, 9201 (1995).
[26] F. Lechermann, F. Welsch, C. Elsässer, C. Ederer, M. Fähnle, J. M. Sanchez, and B. Meyer, Phys. Rev. B **65**, 132104 (2002).
[27] J. P. Perdew and A. Zunger, Phys. Rev. B **23**, 5048 (1981).
[28] H. J. Monkhorst and J. D. Pack, Phys. Rev. B **13**, 5188 (1976).
[29] J. Moreno and J. M. Soler, Phys. Rev. B **45**, 13891 (1992).
[30] C. L. Fu and K. M. Ho, Phys. Rev. B **28**, 5480 (1983).
[31] Y. Umeno, B. Meyer, C. Elsässer, and P. Gumbsch, Phys. Rev. B **74**, 060101(R) (2006).
[32] V. Vitek, Philos. Mag. **18**, 773 (1968).
[33] J. C. Hamilton and S. M. Foiles, Phys. Rev. B **65**, 064104 (2002).
[34] B. S. Thomas, N. A. Marks, and B. D. Begg, Nucl. Instrum. Methods Phys. Res., Sect. B **228**, 288 (2005).
[35] A. Marinopoulos and C. Elsässer, Philos. Mag. Lett. **81**, 329 (2001).
[36] W. Zhong, R. D. King-Smith, and D. Vanderbilt, Phys. Rev. Lett. **72**, 3618 (1994).
[37] R. D. King-Smith and D. Vanderbilt, Phys. Rev. B **47**, 1651 (1993).
[38] R. Janisch and C. Elsässer, Int. J. Mater. Res. **100**, 1488 (2009).
[39] M. Mrovec, C. Elsässer, and P. Gumbsch, Philos. Mag. **89**, 3179 (2009).